Research Article

Josep Arasa*, Carles Pizarro and Patricia Blanco

Simulation of imperfections in plastic lenses – transferring local refractive index changes into surface shape modifications

DOI 10.1515/aot-2016-0024
Received April 15, 2016; accepted June 7, 2016

Abstract: Injection molded plastic lenses have continuously improved their performance regarding optical quality and nowadays are as usual as glass lenses in image forming devices. However, during the manufacturing process unavoidable fluctuations in material density occur, resulting in local changes in the distribution of refractive index, which degrade the imaging properties of the polymer lens. Such material density fluctuations correlate to phase delays, which opens a path for their mapping. However, it is difficult to transfer the measured variations in refractive index into conventional optical simulation tool. Thus, we propose a method to convert the local variations in refractive index into local changes of one surface of the lens, which can then be described as a free-form surface, easy to introduce in conventional simulation tools. The proposed method was tested on a commercial gradient index (GRIN) lens for a set of six different object positions, using the MTF sagittal and tangential cuts to compare the differences between the real lens and a lens with homogenous refractive index, and the last surface converted into a free-form shape containing the internal refractive index changes. The same procedure was used to reproduce the local refractive index changes of an injected plastic lens with local index changes measured using an in-house built polariscopic arrangement, showing the capability of the method to provide successful results.

Keywords: free-form surfaces; index variations; optomechanical design; plastic lenses; polarization.

1 Introduction

In recent years thermoplastic injected lenses have reached the required standard quality to be part of high performance optical systems. Injected lenses are no longer a lower quality product, and they are now included into quality systems and services [1, 2] ranging from automotive applications to the latest generation of optical zooms for mobile telephones [3]. A plastic lens can be manufactured by three different processes. First, it can be cut and mechanically polished from a block of material, as done in conventional glass lenses. In this case, the block of material has not undergone any volume strains, as in the glass case, so the lenses have optical quality equivalent to its glass equivalents. The second possible process is in situ polymerization [typically in e.g. Allyl-diglycol-carbonate (CR39) and equivalent thermostable materials]. This technique is fully in use for ophthalmic lenses, where the monomer is injected at low pressure and the polymer undergoes a polymerization reaction to obtain the final lens. The process is typically slow; usually, they need around 2 h in the best case. The properties of the lens differ from glass lenses because of the density variations inside the lens caused by the polymerization process. Thus, the polymerization time is set to be smooth, typically lasting several hours, so the variations may be done almost negligibly, making these lenses a relevant alternative to glass lenses. Finally, the third process is injection molding, used in thermoplastic lenses [4–6]. Due to the fast solidification process involved, these lenses present the greatest local differences in refractive index in their volume, making them the most relevant candidates for in-line polariscopic quality control.

***Corresponding author: Josep Arasa,** Center for Sensors Instruments and Systems Development (CD6), Universitat Politécnica de Catalunya, Rambla de Sant Nebridi 10, E08222 Terrassa, Spain, e-mail: arasa@oo.upc.edu
Carles Pizarro: Center for Sensors Instruments and Systems Development (CD6), Universitat Politécnica de Catalunya, Rambla de Sant Nebridi 10, E08222 Terrassa, Spain; and SnellOptics™, Carrer Sant Quirze 91,5e2a. E08221 Terrassa, Spain
Patricia Blanco: Center for Sensors Instruments and Systems Development (CD6), Universitat Politécnica de Catalunya, Rambla de Sant Nebridi 10, E08222 Terrassa, Spain

The constituent polymers with thermoplastic properties applied to optics are poly-methyl methacrylate (PMMA), polycarbonate (PC), cyclic-olefin-copolymer, and styrene acrylonitrile. All of them move from solid to liquid state at temperatures between 200°C and 300°C, which is slow enough to make them useful for production purposes. Once in the liquid state they can be injected into a mold, adopting the shape of the cavity, and refrigerated to get back to solid state. The cost of this process is very small, and the material remanent and rejected lenses may be recycled. However, their large advantages regarding their fast and cheap production turn into disadvantages when inaccurate processing turns them into low-quality lenses.

The origin of the problem is the same manufacturing process. The solidification of the thermoplastic induces a fast change from a liquid to a solid state, so a thermodynamic change of state is induced. As the densities of liquid and solid thermoplastic are different, and the time in the transition is very short (usually <5 s), a dynamic, small-scale process in the solidification appears, inducing stress, birefringence, and local changes of density and refractive index.

This dynamic transition starts in the surface in contact with the mold skin and ends inside the core of the lens. Thus, the solidification process of the injected thermoplastic lenses (whether PMMA or PC) involves a volumetric change which affects the refractive index, turning the lens into a gradient index (GRIN) with a particular index profile, which cannot be neglected if quality imaging applications are targeted.

The two main disadvantages of plastic lenses against glass ones are the change of its optical properties with temperature at near-ambient temperatures and its dependence on geometrical shape (thickness being the most relevant factor) [7–10]. There are also some additional dependences to be considered in the parameters linked to the injection process, where internal stress and volume reduction may play a very important role in the final optical performance.

Even in plastic lenses using optimized injection procedures, refractive index presents smooth variations from the internal to the external regions, which appear when the thermoplastic shrinks during the solidification process by introducing variations in shape and surface. This effect is well known since the very beginning of the use of thermoplastics and has so far been considered as a manufacturing defect. Studies on the GRIN profiles induced in injected lenses using the generic injection method [11] and some others propose methods for accurately measuring the induced refractive index variations [12–14].

However, once a good method to estimate the internal refractive index changes is available, a new problem appears when they need to be included in an optical simulation software tool. In this paper we propose a method to include the internal refractive index variations in the lens in simulation tools by transforming them in the equivalent optical path changes and then using this computed optical path difference (OPD) to calculate a free-form surface [15–17], which enables to compensate for the refractive index changes in the lens.

2 Methods

The proposed method intends to provide an equivalent model of the lens to simulate the refractive index variations in the lens. To do so, we will use a lens with homogeneous refractive index and geometric parameters similar to those of the plastic 'GRIN' lens but shaping one of its surfaces with a free-form curve, so the local change in the lens thickness introduces an OPD equivalent to the refractive index variation in the same local coordinates.

The method (see Figure 1) starts with a proposed lens whose shape will be tailored to reach the behavior of the GRIN lens. This lens including the free-form surface will be named from now on the 'final lens'. At its initial stage, it has the same geometrical parameters of the initial lens; the plastic 'GRIN' one, but the material of the lens shows a homogenous refractive index. In the next step the wavefront leaving the initial and the end lenses are calculated. Such wavefront computation, or measurement, needs be carefully done in the same plane, as it is in this plane where they will be compared in the next step.

The local OPD difference between the wavefronts at that plane may then be calculated and used to obtain the local sags of the surface assuming a homogeneous refractive index, which will be added/subtracted to the final lens. When this OPD is added/subtracted to the final lens, the same wavefront expected from the initial lens in the selected wavefront plane will be obtained. To use the second surface of the final lens as the plane where the OPD is computed is the best option, as in these conditions the OPD can be directly translated to thickness changes, by just dividing the optical path changes by the value of the refractive index.

The last step of the method is a fitting process to generate a new, continuous surface for the end lens, which can be carried out using a simple two-dimensional fit if the OPD is rotationally symmetrical, or, in the more general case, fitting will be three-dimensional and a free-form surface will be obtained. Our proposal is to use B-spline curves [18] to fit such a surface, as usually the refractive index variations which appear have no observable symmetry.

3 Results

Results are presented in two subsections. In the first subsection we apply the method on a commercial GRIN lens of known index profile, so in this case we have the analytical expression of the GRIN profile, and the method may be

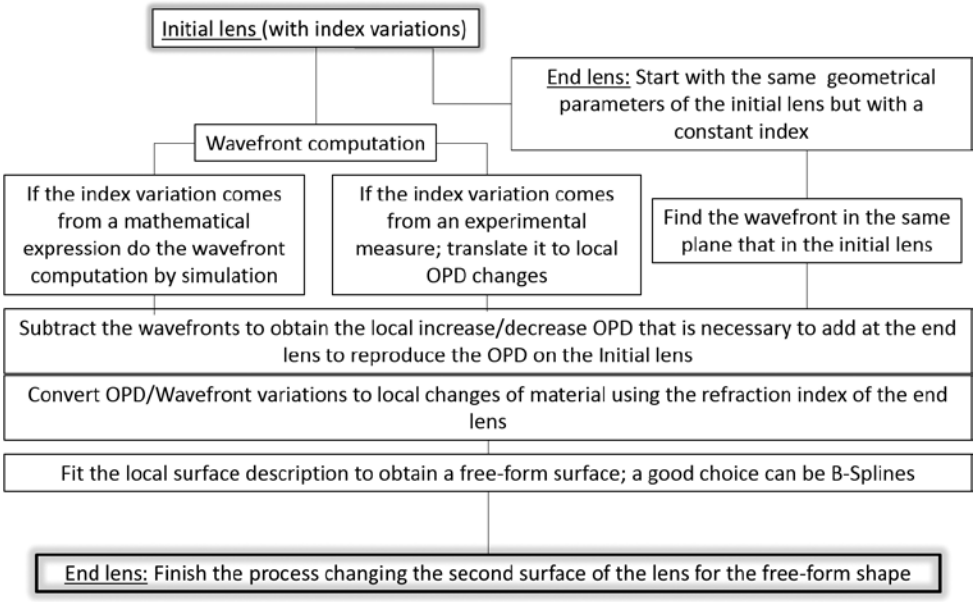

Figure 1: Flux diagram of the method to replace the second surface of a lens with homogenous refractive index with a free-form surface, so the wavefront obtained is equivalent to one obtained in the original lens with a gradient distribution.

tested in full. In the second subsection the method has been applied to a plastic lens manufactured by injection molding and measured using an in-house polariscope to obtain the residual local refractive index variations. Results in the second section may not be validated as there is no refractive index model to be included in the software simulation tool.

3.1 GRIN lens with known refractive index profile

The proposed method calculates a free-form shape in a homogenous index lens out of the optical behavior of a commercial GRIN lens with known index profile. The selected lens was chosen from the commercial catalogue of LightPath™ [19] technologies with reference GPX-10-30. The analytical expression of its profile is described as

$$n=\sum_{i=0}^{11} n_i \left(\frac{z+\Delta z}{z_{\max}} \right)^i \quad (1)$$

Being in the refractive index value along Z axis; z the coordinate value along the lens axis where n will be computed, and Δz the step used during the simulation. For this lens z_{max}=9.4 mm and the n_i numerical values are presented in Table 1. The main optical features of the lens are presented in Figure 2. The aperture stop of the lens is

Table 1: Refractive index values obtained at different axial points of the lens.

i	n_i	i	n_i
0	1.7758298E+000	6	9.2133053E+001
1	-6.3476076E-002	7	-5.3438915E+001
2	6.8687048E-001	8	-2.4823518E+001
3	-6.7605889E+000	9	6.8676506E+001
4	2.8904287E+001	10	-4.8879704E+001
5	-6.9313554E+001	11	1.2759259E+001

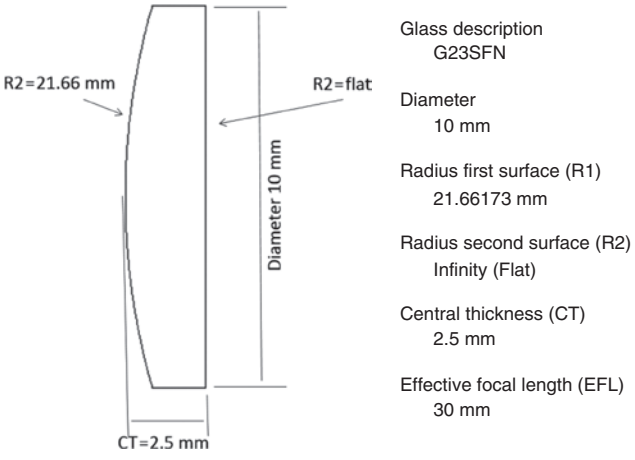

Figure 2: Scheme and main optical parameters of GPX-10-30 from LightPath™.

placed on the second surface. Under these conditions the OPD for an object at infinity is evaluated using Zemax™ [20] (Figure 3A) obtaining a maximum OPD value of 0.035 λ (at 546 nm) in the exit pupil, which has a diameter of 10 mm.

As the final lens we will calculate one with the same geometrical parameters of the initial lens (Figure 2) but changing the glass description to a constant refractive index of 1.760101. The OPD of this new lens is presented in Figure 3B and has been chosen as the standard lens for our development. The OPD images are enough to show that the homogenous refractive index lens does not have the same optical behavior of the initial lens. Such differences may be easily appreciated from the tangential cuts of OPD in Figure 4A and B.

The next step is to subtract the sagittal cuts of the OPDs obtained from the initial and final lenses and use the difference to create a free-form shape which yields a final wavefront equivalent to that of the initial lens.

The final lens has the same geometrical parameters as the initial lens presented in Figure 2, but the GRIN profile has been replaced by a constant refractive index lens with an *ad hoc* local thickness distribution (see Figure 5) to yield an equivalent wavefront shape. A fitting procedure of local thickness was performed to obtain an analytical form from the simulated values obtained with Zemax. The target function was

$$z = ar^4 + br^2 \text{ where } r^2 = x^2 + y^2 \tag{2}$$

where z is now the height of the OPD surface taking as origin the apex of the OPD surface, and x and y are the coordinates of the plane normal to the optical axis. Using a least squares method [21] strategy to find the coefficients of Equation (2), we obtain a value of $a = 1.0179 \times 10^{-5}$ mm^{-3} and a value of $b = 1.8470 \times 10^{-6}$ mm^{-1}, with a correlation coefficient (r^2) of 1.000, meaning the equation passes on all data values. As data are not experimental, error bars or further statistical analysis is not required.

Now we can compute again the OPD in the same plane (see Figures 3C and 4C). Note that the obtained OPDs are not exactly equal; at the border of the OPD function, in the 4–5 mm distance from the center, OPD values decrease, where they were expected to stay at top values. Deviations, however, are around 0.005 λ of the initial lens. Such differences will be seen to be not relevant for our proposal; see, for instance, the spot diagrams of Figure 7.

In order to set and extra accuracy test of the method, the MTF sagittal plots of initial and final lenses until a 400 l/mm frequency for an object placed on axis and at infinity were calculated (Figure 6). Table 2 completes the

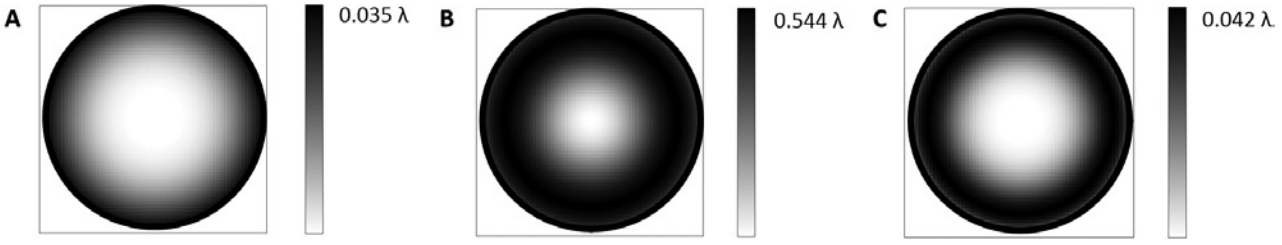

Figure 3: OPD at the exit pupil (second surface of the lens) at λ=546 nm, grey scale of OPD in λ, box dimensions 10×10 mm. (A) Initial GRIN lens GPX-10-30. (B) Final lens when the GRIN profile is changed by a constant index of 1.760101. (C) Final lens with constant index and a second free-form surface added.

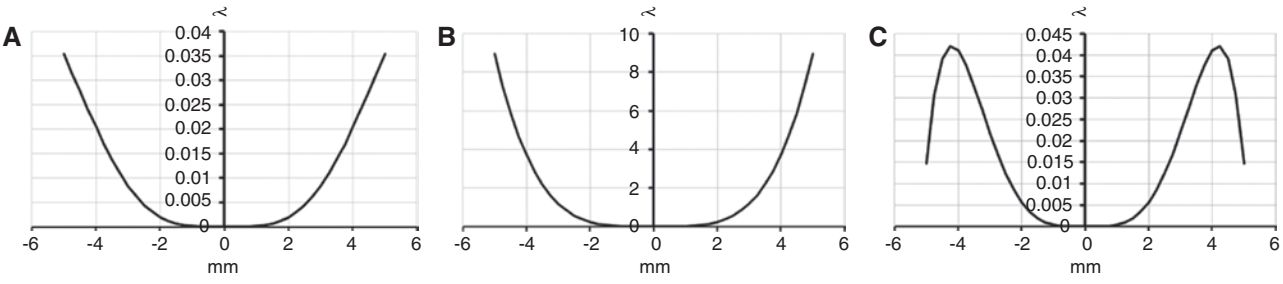

Figure 4: Sagittal cuts of the OPD in the exit pupil, placed on the second surface of the lens at λ=546 nm, vertical scale in λ, horizontal scale in millimeters. (A) Initial lens GPX-10-30. (B) Final lens with GRIN profile replaced by a constant index of 1.760101. (C) Final lens with the free form shape added at the second surface.

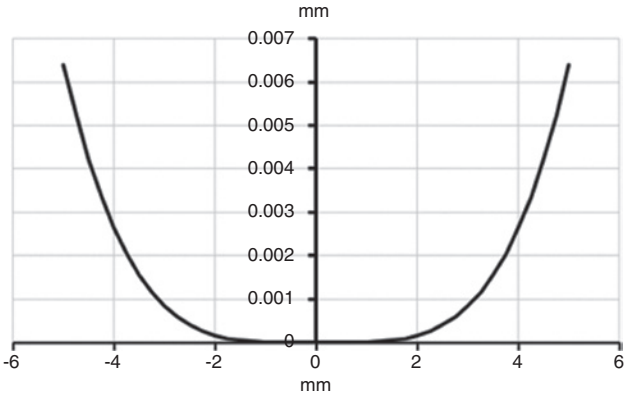

Figure 5: Local thickness distribution in the second surface of the final lens to obtain an equivalent optical behavior. The graph reproduces a sagittal cut (y=0), with X axis in the horizontal and Z axis in vertical. Scales are in millimeters.

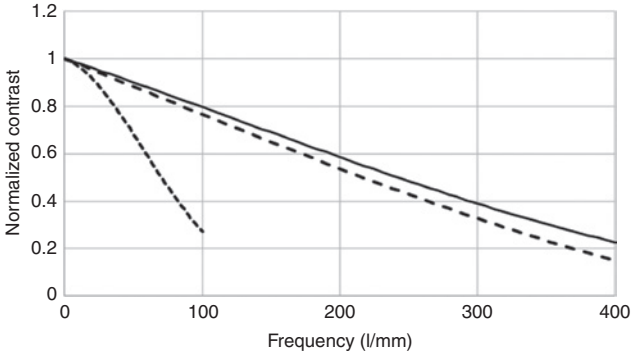

Figure 6: Sagittal MTF representation up to a frequency of 400 l/mm for the initial lens (solid line) and final lenses (long dash line). In the graph are also shown the MTF values of the final lens without the inclusion of a free-form surface (short dash).

Table 2: RMS values of the spot diagrams for the initial and end lens. To do this comparison, the image plane was always refocused to obtain the minimum RMS value for the axis position of the object.

ID	Object placed at	Field value	RMS spot radius (μm)	
			Initial lens	Final lens
1	Infinity	Axis	0.025	0.465
2	Infinity	5 degrees	35 745	44 351
3	5 times EFL	Axis	2754	2718
4	5 times EFL	10 mm high	29 379	34 939
5	2 times EFL	Axis	22 055	28 488
6	2 times EFL	5 mm high	111 659	132 540

comparison of the initial and final lenses with a table presenting the RMS values of spot size for different object positions. It is relevant to notice how both the values on axis and at full field are of comparable magnitude in both lenses.

The set of spot diagrams corresponding to the objects described in Table 2 are presented in Figure 7. The degree of accuracy in the reproduction of optical performance between the Initial and final lenses is presented, showing the feasibility to substitute a GRIN lens with a lens with constant index with a free-form second surface, in this case described by a 4th degree polynomial equation.

3.2 Free-form adjustment for an experimental refractive index change

In this case we start from an injected molded PMMA meniscus lens made in ASCAMM (a technological center devoted to plastic manufacture in the Barcelona area, http://www.ascamm.com). Figure 8 presents the geometrical parameters of the manufactured lens, and Figure 9 shows the lens itself and the tool used. The measurements of the local refractive index variations were done using an in-house built polarimeter based on a transmissive polariscopic arrangement shown in Figure 10.

In the polarimeter, a collimated light beam illuminates the sample lens, which is dipped in a liquid with matching refractive index. The light crossing the sample is collected with an afocal system and its image recorded on a CMOS image sensor. The selection of an afocal system enables to capture the image keeping the same lateral magnification when small changes in the sample position are introduced. The experimental device, shown in Figure 10, comprises a vertical stage and several perpendicular plates where different elements are assembled. The entire device is controlled by a laptop computer which can manage the LEDs for illumination, the stage motors, and the CMOS camera.

The original optical behavior of the lens measured with the setup in Figure 10 can be seen in Figure 11, where a 2D map of the OPD is shown (Figure 11A) and a sagittal cut of the OPD is also presented (Figure 11B).

In these conditions we can also apply the method proposed before. We start from the measurements of the polarimeter which provides us with a local refractive index variation map of the lens (Figure 12). The local changes are in 2.4e-10 units, which can be directly translated into an OPD map by multiplying the difference in refractive indexes by the local thickness of the lens (Figure 13A).

Out of the local variations of the second surface of the lens, a free-form surface was computed to compensate them and fitted to an analytical surface; in our case a uniform and symmetrical B-spline description was used [22]. The free-form surface was obtained on a regular grid of 10×10 control points which covers all the optical area (Figure 14).

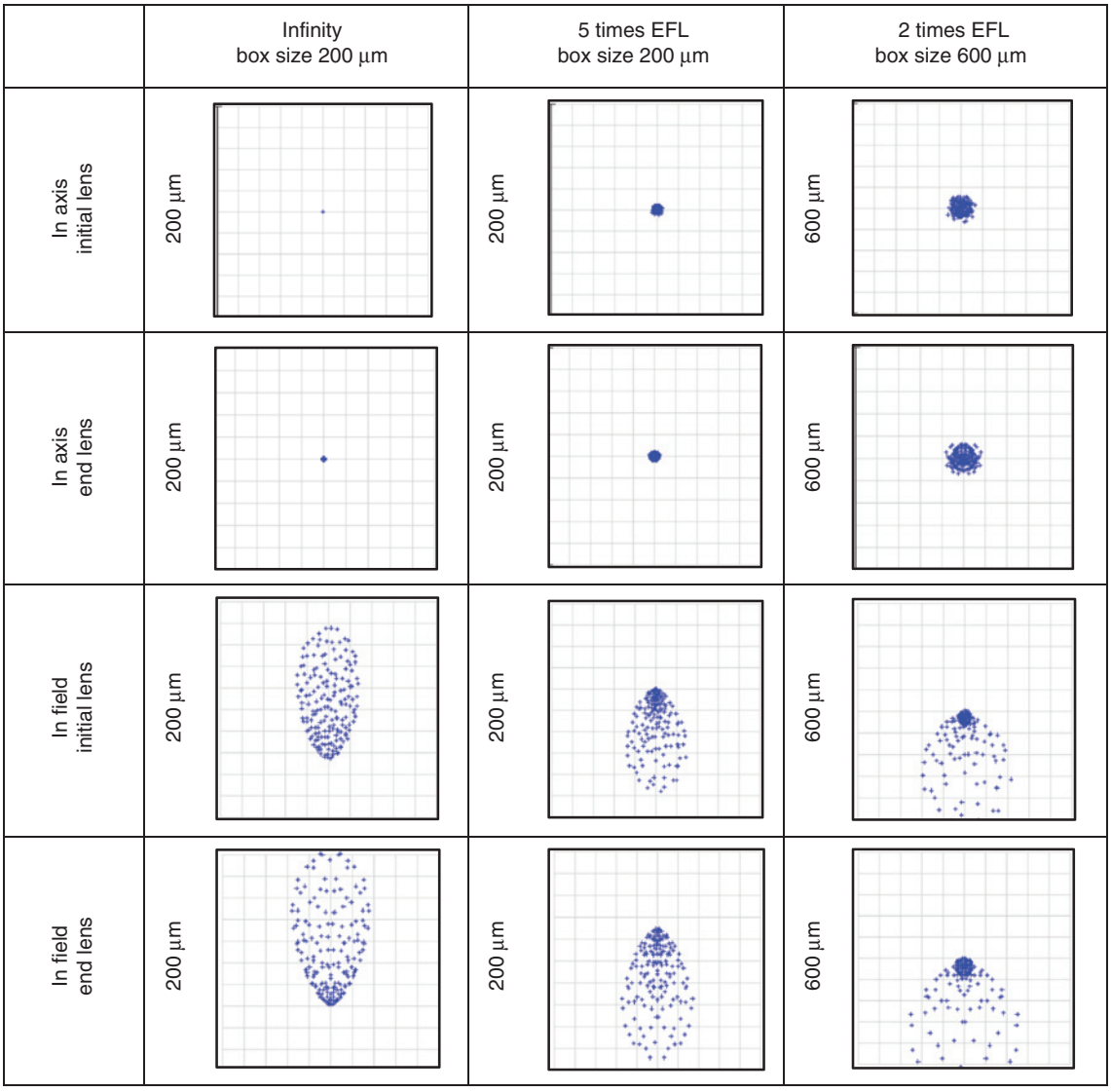

Figure 7: Spot diagrams for the initial and final lenses. Box size is 200 μm for the infinity and 5 times effective focal length (EFL) cases and 600 μm for 2 times EFL. In all the cases the size and structure of the spots are similar, showing an equivalent optical behavior.

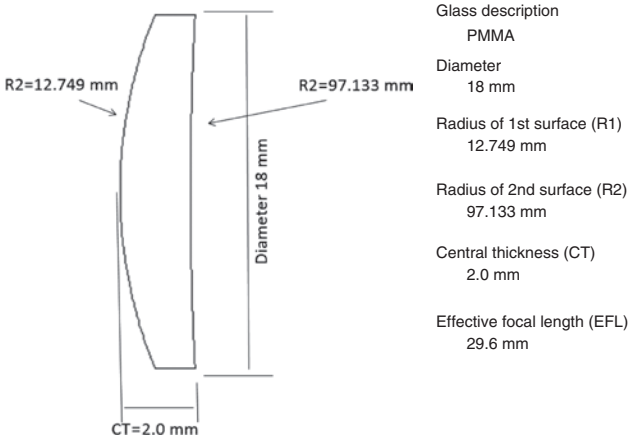

Figure 8: Optical specifications of the injected lens.

As the free-form surface of the final lens must be obtained by fitting, a merit function and an optimization strategy need to be defined. In our example the merit function was set so the absolute difference between the original values, and the values of the fitted surfaces were <0.01 μm in all the points used for the fitting.

$$MF = \text{abs}(\text{dist}((\text{raw data})-(\text{surface data})))<0.02 \quad \text{for } \forall \text{ data values} \tag{3}$$

In order to shorten the computation time in the fitting of Equation (3), only a quarter of the 586 000 useful experimental points collected in the optical area were used.

As important as the merit function selected, it is the optimization strategy used to find the best positions of the

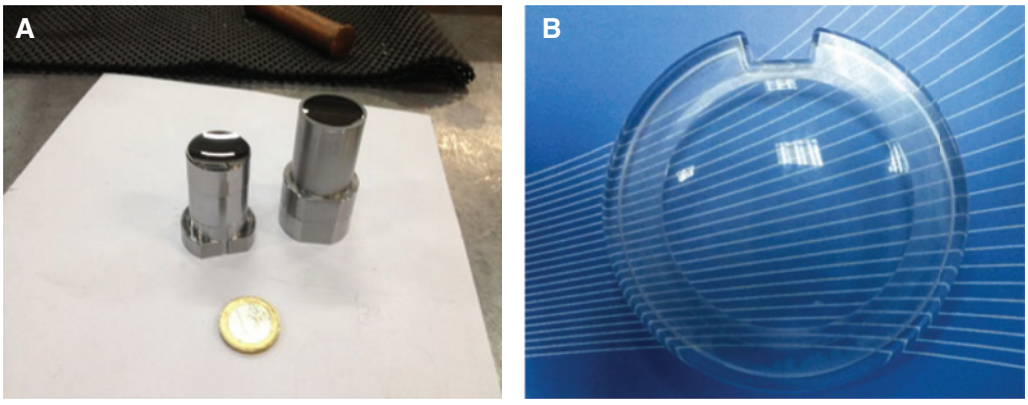

Figure 9: (A) Optical parts of the mold used to inject the sample lens; (B) obtained lens; the ring around the central part is for mechanical support purposes.

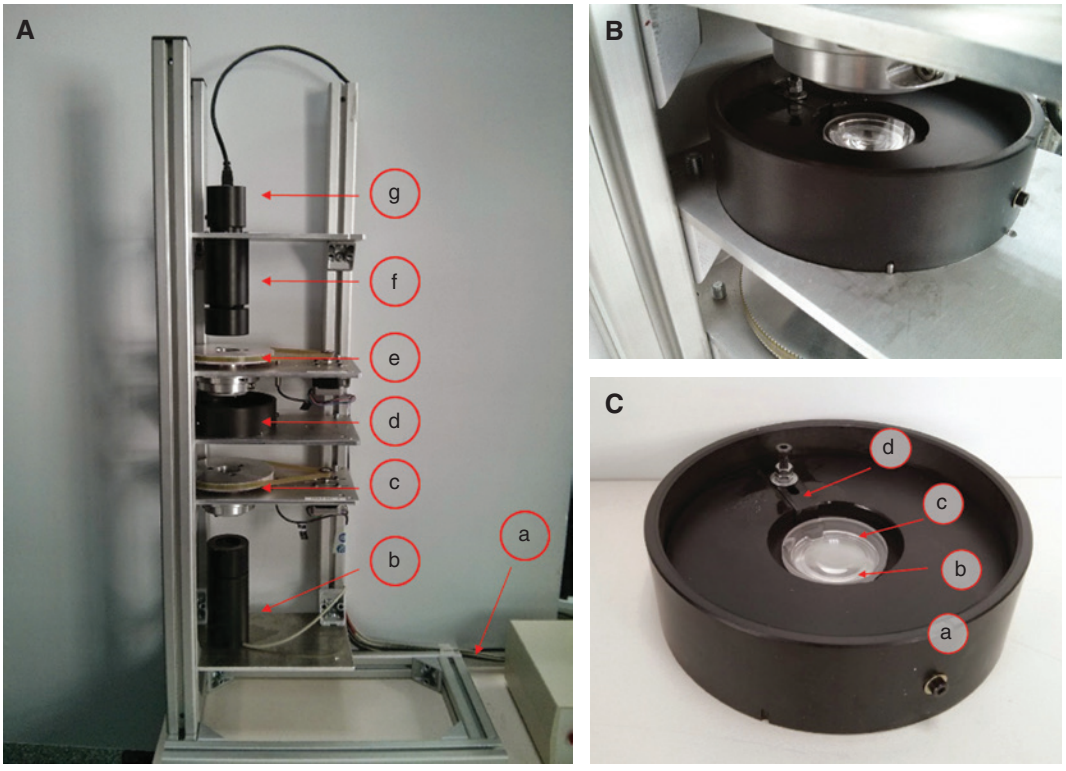

Figure 10: Picture of the experimental setup. (A) Polarimetric bench, bottom to top: (a) Wires to connect with controller and laptop computer. (b) Light source, the illumination device uses a LED source at 626 nm (red) that can be electronically switched and a 100 mm effective focal lens to collimate the light. (c) Polarizer rotation stage; the orientation of the polarizer is also controlled from the laptop. (d) Cuvette, more in detail in Figure 2B and C. (e) Rotation stage for the analyzer, as the orientation of the analyzer is also controlled from the laptop. (f) Afocal imaging system to ensure a constant magnification under small errors in positioning. (g) CMOS sensor. (B) Detail of the cuvette in the polariscopic bench. (C) Structure of the cuvette; (a) holder, the bottom part is on borosilicate; (b) lens under test placed inside the cuvette; the cuvette here is empty, otherwise it is not possible to see it; (c) cover of the cuvette – flat window of N-BK7 glass; (d) fixation of the cover; (B) and (C), detailed view of the setup.

control points; in our case we have used a simplex algorithm strategy [23, 24]. Table 3 presents the z coordinates of the control points used to describe the surface using B-spline description. Coordinates x and y are linked to the cell position, where each cell corresponds to an incremental step of 1.8 mm, which contains a variable number of experimental points. Table 4 presents the residual errors of the fitting process, with the values shown in each cell

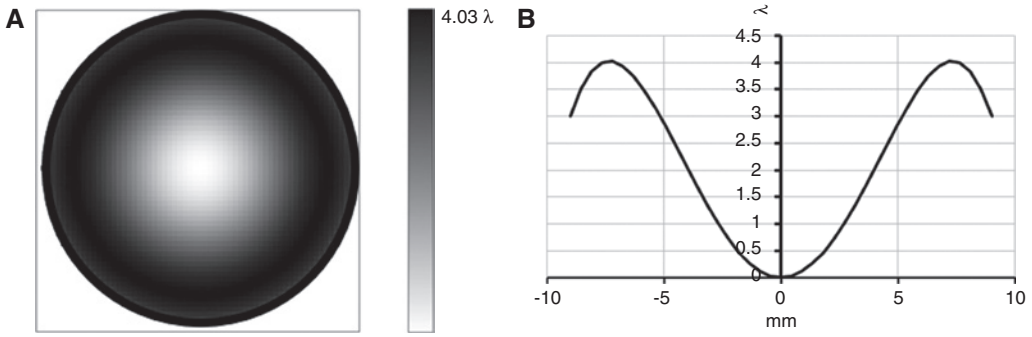

Figure 11: OPD of the manufactured lens for an object placed at infinity and with a wavelength of 626 nm. (A) 2D map, box dimensions 18×18 mm. (B) Sagittal cut, vertical scale in wavelength units and horizontal scale in millimeters.

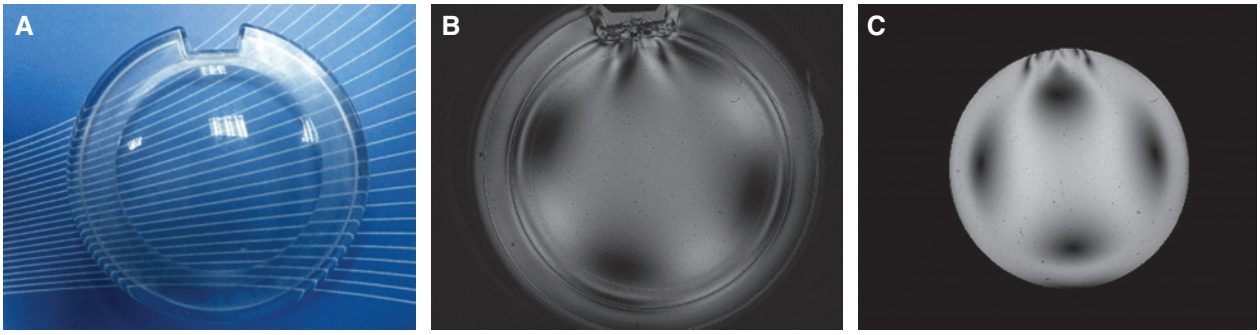

Figure 12: (A) Injection-molded lens provided by ASCAMM. The optically active area has a diameter of only 9 mm, with the surrounding area used to fix the lens in the holder. (B) One of the measurements obtained using the polariscope. (C) Local refractive index differences; the complete image bit depth (black to white) covers 2.4e-10 units of refractive index.

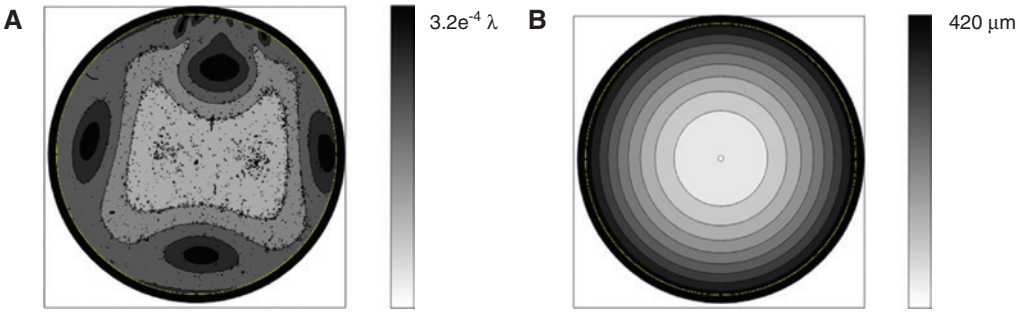

Figure 13: (A) Local changes of OPD measured. (B) New free-form surface generated using the measured local variations of OPD; size of the box is 18×18 mm.

of the table corresponding to local differences between the average value of the fitted surface (described using B-splines) and the average value of the sample points in the same cell. Such residual values are presented on the lens diameter in Figure 15, showing fitting errors below 0.01 µm in all cases.

Thus, the injected molded lens, which presented uncontrolled changes of refractive index due to the manufacturing process used, can now be exchanged with this lens of equivalent performance, with the second surface replaced by a free-form shape easy to implement in further optical simulations.

In this particular example the values of the induced changes in the refractive index were below the minimum amount relevant to noticeably impact the shape of the second surface. To validate the proposed method, we artificially raised two orders of magnitude the weight of the internal changes in refractive index, so the effect in the

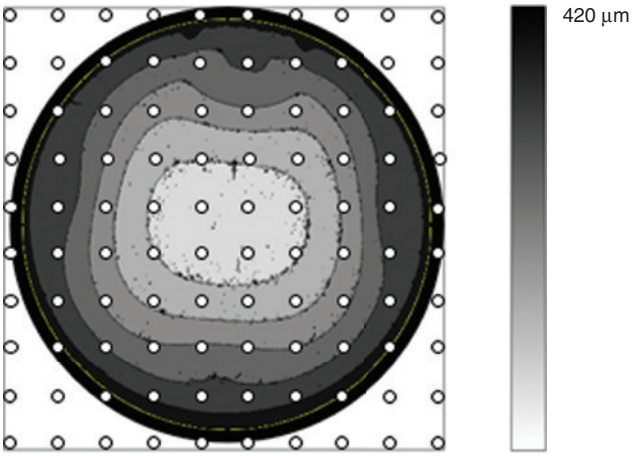

Figure 14: Control points for B-spline adjustment. The figure presents the points superimposed to the 2D representation of the second surface of the lens; size of the box is 18×18 mm.

final free-form surface was noticeable. It is stressed that such change in scale does not affect the validity of the proposed method.

4 Conclusions

We have proposed a method to model in conventional optical simulation software tools the effects on optical performance of the internal refractive index changes in an injection molded plastic lens. The final lens has a constant refractive index and the same geometrical parameters of the initial lens, but its second surface is replaced by a free-form surface. In the paper we present a method to calculate such free-form surface, and we have applied it to a commercial GRIN lens and to a real PPMA injected

Table 3: Z value (in μm) of the control points of the B-spline used to fit the second surface to the measured local thickness variations.

	1	2	3	4	5	6	7	8	9	10
1	0	0	0	0	423.02	266.76	0	0	0	0
2	0	0	381.67	299.02	257.72	258.25	300.61	384.31	0	0
3	0	381.67	257.72	175.18	133.93	134.46	176.76	260.36	385.37	0
4	0	299.02	175.18	92.70	51.49	52.02	94.29	177.82	302.72	0
5	423.02	257.72	133.93	51.49	10.30	10.83	53.08	136.57	261.42	427.77
6	266.76	258.25	134.46	52.02	10.83	11.35	53.61	137.10	261.95	428.30
7	0	300.61	176.76	94.29	53.08	53.61	95.88	179.40	304.31	0
8	0	384.31	260.36	177.82	136.57	137.10	179.40	263.00	388.01	0
9	0	0	385.37	302.72	261.42	261.95	304.31	388.01	0	0
10	0	0	0	0	427.77	428.30	0	0	0	0

A uniform and symmetrical B-spline description was used. The X and Y values of the control points were determined for the selected grid sample, which in this case had values going from -9 mm to 9 mm in 10 equally spaced steps. The reference of the B-spline control points is taken on a plane perpendicular to the Z axis and tangent to the apex of the second surface of the lens.

Table 4: Residual values when a uniform and symmetrical B-spline description was used to fit the surface.

	1	2	3	4	5	6	7	8	9	10
1	0	0	0	0	0.00998	0.00989	0	0	0	0
2	0	0	0.00584	0.00672	0.00720	0.00716	0.00665	0.00576	0	0
3	0	0.00587	0.00719	0.00797	0.00857	0.00849	0.00813	0.00733	0.00585	0
4	0	0.00672	0.00802	0.00892	0.00961	0.00954	0.00910	0.00798	0.00674	0
5	0.00993	0.00716	0.00854	0.00952	0.01004	0.01008	0.00957	0.00867	0.00731	0.00983
6	0.00981	0.00709	0.00849	0.00962	0.01003	0.01009	0.00953	0.00860	0.00717	0.00984
7	0	0.00670	0.00817	0.00918	0.00960	0.00961	0.00903	0.00811	0.00680	0
8	0	0.00571	0.00730	0.00808	0.00872	0.00865	0.00804	0.00725	0.00580	0
9	0	0	0.00584	0.00688	0.00708	0.00725	0.00672	0.00588	0	0
10	0	0	0	0	0.00986	0.00982	0	0	0	0

All values are below 0.01 μm and positive due to the merit function used in the fit. First row and first column are the cell number of the X and Y values of the control points were determined for the selected grid, which in this case had values going from -9 mm to 9 mm in 10 equally spaced steps.

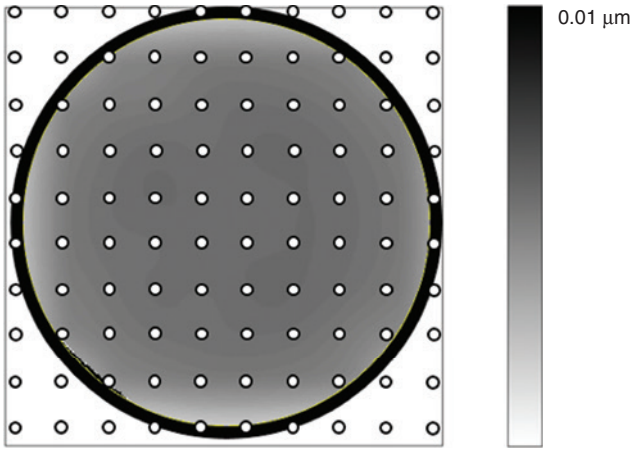

Figure 15: Residuals of the fitting in the selected control points. Numerical values can be found in Table 4. Points (in white) are superimposed to the surface.

molded lens whose internal refractive index variations have been measured using an in-house built polarimeter.

Acknowledgments: This work has been financed by the 'Spanish Ministerio de Economía y Competitividad' grant DPI2012-38647-C02-01.

References

[1] Thorlabs, generic optical supplier, Available at: http://www.thorlabs.de/newgrouppage9.cfm?objectgroup_id=16.
[2] G-S plastic Optics, plastic optic supplier, Available at: http://gsoptics.com/product/index.php.
[3] K. Matsusaka, S. Ozawa, R. Yoshida, T. Yuasa and Y. Souma, Proc. SPIE 6502, 650203 (2007).
[4] Ledil, plastic optic supplier, Available at: http://www.ledil.fi/.
[5] Neotronic, illumination supplier, Available at: http://www.neotronic.com/EN/kathod-lenses-for-power-leds.html.
[6] Carclo, plastic optic supplier, Available at: http://www.carclo-optics.com/.
[7] P. Obreja, P. Cristea, A. Dinescu and R. Rebigan, Proc. Eur. Opt. Soc. Annu. Meet. 2010 (EOSAM 2010) (Parc Floral de Paris, France, 2010).
[8] D. Cristea, P. Obreja, A. Dinescu, G. Konstantinidis, R. Rebigan et al., Proceedings of 4M Conference,- eds. B.Fillon, C.Khan-Malek, S. Dimov, Research Publishing, 263–266 (2010), doi:10.3850/978-981-08-6555-9.168.
[9] M. Kusko, C. Kusko and D. Cristea, 2nd EOS Conference on Manufacturing of Optical Components (EOSMOC 2011) at the World of Photonics Congress, Munich, Germany, 23–25 May 2011.
[10] P. T. Tang, R. Sobiecki, M. Hansen, C. Ravn and C. Baum, ICOMM proceedings, Tokyo, March 2011, pp. 431–435.
[11] H. Suhara, Appl. Opt. 41, 5317–5325 (2002).
[12] Y.-L. Chen, H.-C. Hsieh, W.-T. Wu, W.-Y. Chang and D.-C. Su, Appl. Opt. 49, 6888–6892 (2010).
[13] J. Arasa, D. Mayershofer and J. Romero, Proc. SPIE 9525, ISBN: 9781628416855 (2015).
[14] N. Domínguez, D. Mayershofer, C. Garcia and J. Arasa, Opt. Eng. 55, 024102 (2016).
[15] G. Farin, 'Curves and Surfaces for CAGD' 5th ed. (Morgan Kaufmann, San Francisco, 2002).
[16] P. Jester, C. Menke and K. Urban, Appl. Opt. 50, 822–828 (2011).
[17] B. Narasimhan, P. Benitez, J. C. Miñano, J. Chaves, D. Grabovickic, et al., Proc. SPIE. 9629, Optical Systems Design 2015: Illumination Optics IV, 96290C. (2015) doi: 10.1117/12.2190882.
[18] G. Farin and D. Hansford, 'The essentials of CAGD' (AK Peters, Ltd. Publishers 2000).
[19] LightPath Technologies, 2603 Challenger Tech Court, Suite 100, Orlando, USA, Available at: http://www.lightpath.com/.
[20] Zemax, LLC, 10230 NE Points Dr. Suite 540, Kirkland, WA 98033 USA, Available at: http://www.zemax.com/.
[21] S. C. Chapra and R P. Canale, 'Numerical methods for engineers' 6th ed. (McGraw-Hill, New York, 2010).
[22] C. de Boor. 'A practical guide to splines' (Springer Verlag, New York, 2001).
[23] J. A. Nelder and R. Mead, Comput. J. 7, 308–313 (1965).
[24] Y. S. Kim and 'Refined simplex method for data fitting' Astronomical Data Analysis Software and Systems VI, A.S.P. Conference Series, Vol. 125, Eds. Gareth Hunt and H. E. Payne (1997) p. 206.